In vivo harmonic generation microscopy for monitoring the height of basal keratinocytes in solar lentigines after laser depigmentation treatment

PEI-JHE WU,[1,2] SHENG-TSE CHEN,[1] YI-HUA LIAO,[3,4] AND CHI-KUANG SUN[1,2,*]

[1]*Department of Electrical Engineering and Graduate Institute of Photonics and Optoelectronics, National Taiwan University, Taipei 10617, Taiwan*
[2]*Molecular Imaging Center, National Taiwan University, Taipei 10617, Taiwan*
[3]*Department of Dermatology, National Taiwan University Hospital and National Taiwan University College of Medicine, Taipei 10002, Taiwan*
[4]*yihualiao@ntu.edu.tw*
[*]*sun@nu.edu.tw*

Abstract: The development of solar lentigines (SLs) is related to chronic ultraviolet exposure-induced cell senescence. We have previously demonstrated that basal keratinocyte enlargement is a morphological hallmark of skin senescence correlated to the process of skin aging, while clinical studies on the long-term monitoring of the cellular morphological changes in SLs after laser treatment are lacking. In this study, we have developed the harmonic generation microscopy (HGM) for *in vivo* monitoring the height of basal keratinocytes (HBK) and had administered Q-switched ruby laser or picosecond 532-nm Nd:YAG laser treatment on each side of the face of 25 Asian patients with facial SLs, respectively. *In vivo* HGM imaging was conducted to longitudinally analyze HBK and the horizontal cell size (HCS). Before treatment, the HBK was significantly higher in the SLs lesional area than that in the adjacent normal region, whereas there was no significant difference in the HCS. After treatment, the lesional HBK remained significantly higher than normal skin regardless of the laser treatment used. Our study indicates that the basal keratinocytes remain abnormal after laser treatment and demonstrates the capability of *in vivo* HGM for longitudinal, quantitative monitoring of cell senescence and therapeutic effect in SLs.

1.   Introduction

Solar lentigines (SLs) are well-demarcated brownish macules found especially on the sun-exposed/photoexposed skin [1]. It is a common hyperpigmentary skin disease, occurring with an extremely high prevalence of approximately 90% among older Caucasians and 70% among Asians and thus has resulted in a high demand for cosmetic treatment [2]. One therapeutic option for skin pigmentation conditions is laser treatment, with the Q-switched ruby laser (QSRL) being particularly successful in the removal of pigmented lesions and having a relatively lower rate of adverse events among all melanin-selective QS lasers [3–6]. Recently, the picosecond laser has also been applied in the treatment of SLs [7]. Although laser depigmentation treatments appear to be effective for removing the accumulation of melanin, their long-term efficacy in treating SLs is not as perfect, and the underlying pathogenesis of SL remains unclear [8–10]. To investigate these issues clearly, treatment assessment should rely on histopathological examinations rather than on clinical evaluations based on the photographic records of skin appearance.

Despite the fact that the mechanisms of SL development remain unclear, it is well known that chronic sun or ultraviolet radiation exposure stimulates melanosome transfer and causes the

deposition of melanin in basal cells, which are the critical factors for the pathogenesis of SLs [11,12]. A recent study had indicated that skin senescence contributes to the development of SLs [13]. Shin et al. [14] pointed out that immunostaining for p16, a marker of senescence, was positive in facial skin biopsy samples from Asian patients with SLs, suggesting the involvement of this cellular process in this skin condition. Moreover, a comparative quantitative analysis of basal keratinocytes revealed the aging cells to be larger in size than the younger cells [15], which probably results in a higher melanin burden. Thus, enlarged keratinocytes could be a morphological hallmark of senescence in SL lesions. However, to the best of our knowledge, the histopathological studies of SLs in the literature have mostly focused on the observation of melanin clearance after laser treatment, and there are no studies that have completely investigated the morphological changes in basal keratinocytes in SLs.

Currently, the histopathological examination of skin biopsies is the gold standard for the evaluation of cellular morphological changes in dermatological studies. However, the use of skin biopsies has several limitations, such as its invasive nature and unsuitability for the study of cosmetic disorders as well as the incapability of following the treatment outcome on the same spatiotemporal points longitudinally. By contrast, stain-free, label-free, real-time *in vivo* imaging techniques would allow the observation of histopathological changes in human skin, provide images with microscopic details for both quantitative and qualitative analyses, and facilitate the long-term tracking of the same sites.

In this study, we first showed that by combining *en face* harmonic generation microscopy (HGM) images optically sectioned at different depths, one can accurately determine the height of basal keratinocytes (HBK). HGM was then applied *in vivo* for long-term monitoring of the histological characteristics of basal keratinocytes in patients with SLs, before and after two types of laser treatments, in order to elucidate the pathogenesis of the disease. The morphological parameters examined include not only the HBK but also their horizontal cell size (HCS). To avoid bias from the specific laser treatment, each recruited patient received two types of laser treatment; one facial side was treated with QSRL and the other side was treated with picosecond Nd:YAG laser (PSNYL). The reliability of the HGM system for measuring the HBK and HCS was histologically validated through *ex vivo* analysis. Our findings support the use of *in vivo* HGM for the long-term monitoring of SLs treatment and suggest that basal keratinocytes remain abnormal long after laser treatment.

2. Experimental section

2.1. Study population

This prospective clinical trial was conducted according to the Declaration of Helsinki and approved by the research ethics committee of the National Taiwan University Hospital (no. 201612113DINC). Asian patients with SLs on the face were recruited for the study. We excluded subjects who had chronic inflammation on the face, previous treatment on the lesions, pregnancy or breastfeeding, and frequent sun exposure (>4 h per day). In total, 25 patients (1 male and 24 females; age range: 46–78 years) with Fitzpatrick skin phototype III or IV and having SLs lesions of at least 4 mm on both sides of the face were enrolled after informed consent had been obtained. The *in vivo* HGM imaging was performed at the Molecular Imaging Center of National Taiwan University.

2.2. Laser treatments

All patients received laser treatment at the Department of Dermatology, National Taiwan University Hospital. First, a split-face area was delimited on each patient. Then, one facial side was treated using a 694 nm QSRL (Sinon; WaveLight, Erlangen, Germany), with a spot size of 5 mm, fluence of 5.5 J cm^{-2}, and speed of 1 Hz over a single pass. The laser pulsewidth was 20 ns.

The other facial side was treated using a 532 nm PSNYL (Picoway; Syneron Candela, Irvine, CA, USA) with a spot size of 4 mm, fluence of 0.5–0.6 J cm^{-2}, and speed of 1 Hz over a single pass. The laser pulsewidth was 375 ps. All patients were instructed to apply 1% tetracycline hydrochloride ointment to the treated areas twice daily until the crusts had peeled off. The use of sunscreen with a sun protection factor of 50+ as well as sun avoidance throughout the study period was requested.

2.3. Harmonic generation microscopy (HGM)

In HGM, the central wavelength of 1262 nm not only is located within the transmission window of human skin but also avoids absorption by melanin and skin scattering, thus allowing a penetration depth of more than 300 μm [16]. A schematic of the *in vivo* HGM system for the clinical trial is shown in Fig. 1. A 1262 nm Cr:Forsterite laser [17], with a 105 MHz repetition rate and 91 nm bandwidth, was used as the excitation source, and double-chirped mirrors were applied to control the optical dispersion [18–20]. The laser beam was collimated, and its size was reduced by a telescope at the same time and light-guided (1.25 Series Laser Articulated Arms; LaserMech, Michigan, USA) into galvo-resonant mirrors (Laser Scanning Essentials Kit; Thorlabs, Newton, NJ, USA) to perform 2D scanning. For the acquisition of high-resolution images, a 1.15 numerical aperture objective (40×; working distance: 250 μm; UApo N 340; Olympus, Tokyo, Japan) was used to focus the laser beam onto the skin. The backward epi-second harmonic generation (epi-SHG: ~630 nm) and epi-third harmonic generation (epi-THG: ~420 nm) signals were collected from each *en face in vivo* skin image using the same objective and were received by two separate photomultiplier tubes (R928 for epi-SHG, and R4220P for epi-THG; Hamamatsu Photonics, Hamamatsu City, Japan). The objective was attached to a 3D step motor (TSDM40-15X, Sigma Koki, Japan) such that the position of the objective could be adjusted by both manual and electrical controls. The imaging plane was moved to different depths by tuning the 3D stage along the optical axis. Following a similar pulsewidth measurement and dispersion control [18], the pulsewidth after the objective was estimated to be 28 fs. THG transverse and axial resolutions were approximately 0.4 and 0.7 μm, respectively [16].

2.4. Imaging procedure

All the *in vivo* HGM image stacks were acquired using the same protocol. In brief, the 3D image stacks for each patient were acquired from three different positions on the face, namely, from a normal region and from the SLs lesions on the left and right facial sides. For registration, we took photographic records before and after the HGM imaging. The average power of the laser source after the objective was 100 mW. Moreover, the voltages of the photomultiplier tubes for the epi-SHG and epi-THG modalities were set at 700 and 650 V, respectively. The *en face in vivo* HGM image stacks had a 235 × 235 μm field of view with 512 × 512 pixels. The 14 bit 3D image stacks, each comprising 110 depth-dependent 2D images with two channels, were obtained through the epidermis and upper dermis. In this study, we choose 1.8 μm as the z-step size for optical section. The acquisition time was approximately 0.38 second per averaged image, after averaging 5 frames at a fixed depth with a 15 Hz frame rate. To acquire a 200-μm-depth stack, it took 110 steps (under the 1.8 μm step size) with 40 seconds in total. The allowed acquisition time for one patient was less than 30 min. For photodamage evaluation and discussions, please consult Ref. [21]. In this present study, no erythema, pigmentation, or blister formation was found on the examined skin. Moreover, we adopted a vacuum-pump adaptor [22] to fix and stabilize the relative position of the imaged skin and microscope, to avoid motion artifacts. A representative *en face in vivo* HGM image stack of the normal skin is presented in Fig. 2, beginning from the stratum corneum and through the stratum granulosum, stratum spinosum, stratum basale, and papillary dermis to the upper reticular dermis.
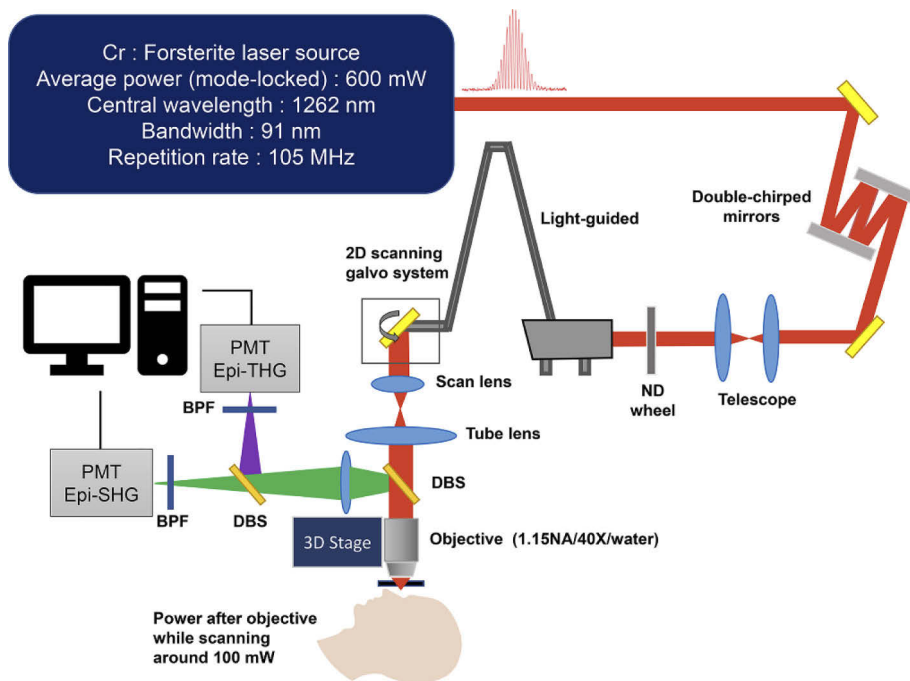
Fig. 1. Schematic showing the 1262-nm-based harmonic generation microscopy system, adapted from a commercial laser scanning system from Thorlabs. BPF: bandpass filter; DBS: dichroic beam splitter; ND: neutral density; PMT: photomultiplier tube.

2.5. Analysis protocols

2.5.1. Height of basal keratinocytes (HBK)

For the quantitative analysis of the HBK, we conducted two inspection procedures to ensure all *in vivo* HGM image stacks with any longitudinal and lateral motion artifact in the imaged basal layers were excluded as being invalid. A preliminary inspection will be performed after we acquired the HGM images immediately. If there was an obvious motion blur, the image stack will be excluded and the HGM images will be acquired again. The second inspection will be performed when analyzing the clinical data, and HGM images with lateral and/or axial motion artifacts in the basal layer were recorded and excluded. Each valid image was divided into nine equal square regions, and one basal cell from each region was randomly chosen for HBK measurement. The basal cells are located in the basal layer (the deepest layer of the epidermis), and the basal layer is only composed of a single layer of basal cells. As shown in Fig. 3, the definition of the first layer of HBK as the layer that the supranuclear melanin cap of the basal cell was firstly seen [Fig. 3(c)] through THG. The definition of the last layer of HBK was the previous layer of a layer that the THG signal of the same basal cell firstly disappeared [Fig. 3(n)]. The number of the last layer from the number of the first layer was then subtracted and multiplied by the z-step size (1.8 μm) of the optical section. Then, the HBK of the represented basal cell for each square region was obtained. The HBK values of the nine cells were then averaged, and the mean HBK for each image stack was acquired. The HBK of each state was the average of three qualified image stacks for each patient.
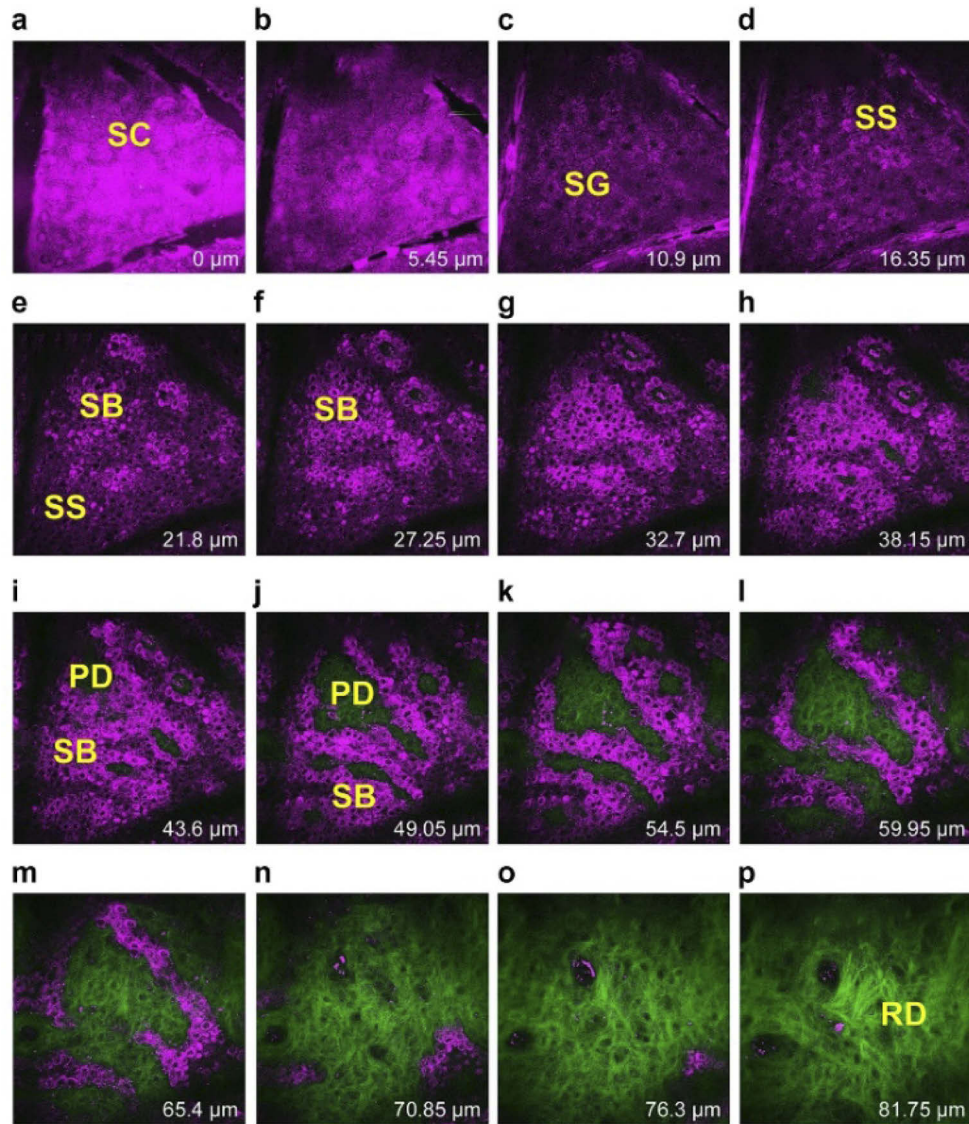
Fig. 2. Representative en face in vivo harmonic generation microscopy image stack of human facial skin at different depths obtained by combining the epi-second harmonic generation (green) and epi-third harmonic generation (magenta) signals. The step size of the horizontal axis of the automatic step motor was 1.84 μm. Scale bar = 50 μm. SC: stratum corneum; SG: stratum granulosum; SS: stratum spinosum; SB: stratum basale; PD: papillary dermis; RD: upper reticular dermis.
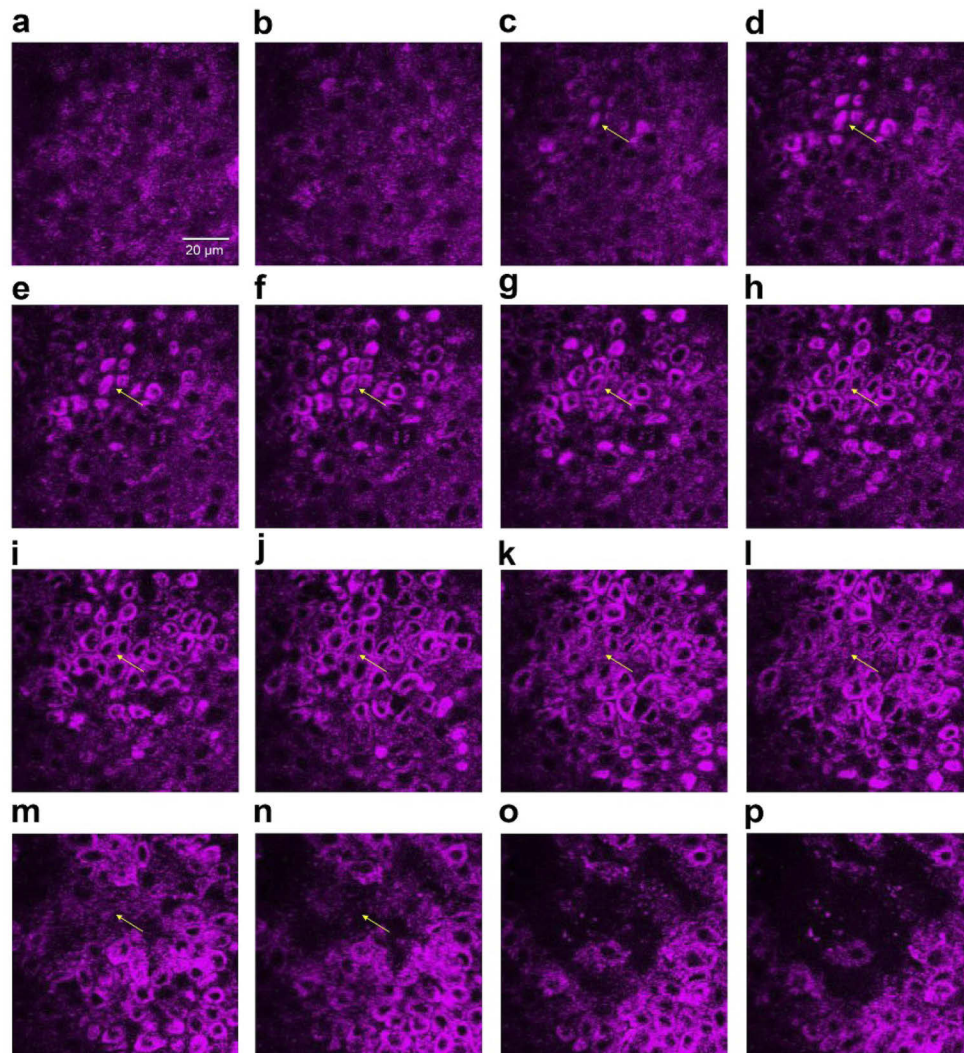
Fig. 3. One representative 3D THG image stack of solar lentigo composed by a series of en face in vivo harmonic generation microscopy images optically sectioned at different depths. From (a) to (p), the plane of observation starts from the suprabasal layer and moves toward the dermis. In (c)–(n), the height of a basal cell (yellow arrow) is shown. Scale bar = 20 μm.

2.5.2.　Horizontal cell size (HCS) of basal keratinocytes

At least three continuous images at the dermal–epidermal junction were randomly selected for each *in vivo* HGM image stack. With a system depth resolution much smaller than the cell height, the observed HCS of a cell would vary with the observation depth. To ensure that the central region, with the widest cell size, of a cell cross-section was chosen, the first 10 cells with the largest cross-sectional area in each image were selected for measuring the cell areas [16,23]. For images with less than 20 segmented cells, only the 5 largest cells were chosen. For each image, the cytoplasm of the basal cell at the innermost layer of the epidermis was segmented and analyzed on the basis of the epi-THG contrast information (Fig. 4). For cell segmentation, please refer to Ref. [24]. Blurred image stacks attributed to motion artifacts or images with fewer than 10 cells segmented were excluded, and manual removal of apparent non-basal cell segmentations was carried out. The HCS of each state was the average from three qualified image stacks for each patient.
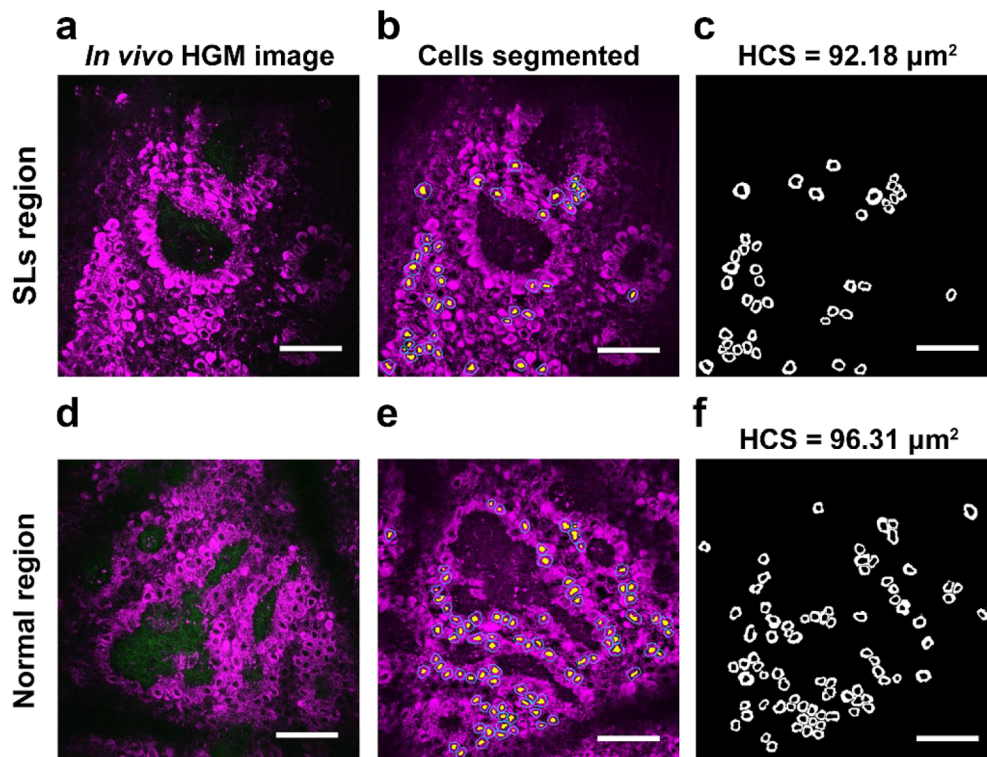

Fig. 4. (a and d) Representative images of harmonic generation microscopy to be analyzed from the solar lentigo (SLs) and normal regions. (b and e) The magenta parts (THG) represent the cytoplasm and the yellow parts surrounded by the segmented cytoplasm are the nuclei. (c and f) The mean of the horizontal cell size (HCS) of the basal keratinocytes from 10 largest cross-sectional areas is 92.18 μm2 in the SLs region and 96.31 μm2 in the normal region. (Reference [24]) Scale bar = 50 μm.

2.6.　*Ex vivo histological validation of the HGM system*

To confirm the reliability of the HGM system for measuring the HBK and HCS in SLs, we conducted an analysis to statistically compare the results between *ex vivo* HGM image stacks and hematoxylin and eosin (H&E) staining images of the same human skin specimen. Fresh

skin tissues were obtained from the National Taiwan University Hospital. This experiment was approved by the research ethics committee of the National Taiwan University Hospital (no. 201804100DINA).

2.7. Ex vivo analyses of the HBK

Two types of tissue samples (normal human thigh skin tissue and normal armpit skin tissue) were obtained and embedded in normal saline under ambient temperature and then immediately investigated. For quantitation of the HBK, five different positions on each skin tissue were randomly selected and *ex vivo* HGM image stacks were acquired. Furthermore, 10-μm-thick continuous transverse sections of frozen or formalin-fixed tissue were obtained and immediately stained with H&E according to standard procedures (conducted at the Laboratory Animal Center, National Taiwan University College of Medicine, Taipei, Taiwan) and observed under a light microscope (CM1950; Leica, Wetzlar, Germany). In total, 200 basal keratinocytes were randomly selected from the *ex vivo* HGM image stacks and statistically analyzed. For the H&E staining images, 234 basal keratinocytes from three different positions were selected, and their heights were measured using ImageJ software (http://rsb.info.nih.gov/ij/), whose source code is freely available and was written by Wayne Rasband at the National Institute of Health (Bethesda, MD, USA).

2.8. Ex vivo analyses of the HCS of basal keratinocytes

Normal armpit skin tissue was obtained and processed further to obtain continuous horizontal frozen sections of 10 μm thickness. Additionally, two frozen sections at the dermal–epidermal junction were randomly selected, and *ex vivo* HGM image stacks were acquired. Furthermore, H&E staining of the same sections was performed and observed under the CM1950 light microscope. In total, 422 basal keratinocytes from the two skin sections were automatically segmented on the *ex vivo* HGM images using the MATLAB program, and the removal of apparent non-basal cell segmentations from the different images was then performed manually. For the H&E staining images, 250 basal keratinocytes were randomly and manually selected using ImageJ software.

2.9. Statistical analysis

All data gathered were subjected to decoding and were analyzed by blinded evaluators using SPSS software (version 20.0; IBM, Armonk, NY, USA). Outliers of the morphological parameters were determined with the SPSS program and were not considered in the statistical analysis. All t-tests were two-sided. A P-value of less than .05 was considered statistically significant.

2.10. Quantitative analysis of en face in vivo harmonic generation microscopy images

En face in vivo HGM image stacks were captured from 25 patients with SLs at three different stages (baseline: before treatment, week 3: 3 weeks post treatment, and week 6: 6 weeks past treatment). The 3-week interval duration was determined by the epidermal turnover time [25]. Two morphological parameters relevant to basal keratinocytes (i.e., HBK and HCS) were then determined from the images.

3. Results

3.1. Ex vivo analysis of the HBK

Validation of the HGM system on the basis of the HBK results was carried out by *ex vivo* imaging and H&E staining using a normal armpit skin tissue and a thigh skin tissue. HBK was determined by a series *en face* horizontal THG images as exemplified in Fig. 3, following the protocol described in 2.5.1. For validation, the HBK height was compared to transverse sectioned H&E

images of the same tissue. A representative H&E staining image is shown in Fig. 5. For the armpit skin tissue, the mean HBK values from the *ex vivo* HGM image stacks and H&E staining images were approximately 15.5 ± 0.7 and 14.5 ± 1.5 μm, respectively, with a percentage error of 6.5%. By contrast, for the thigh skin tissue, the mean HBK values from the *ex vivo* HGM image stacks and H&E staining images were approximately 11.9 ± 1.5 and 11.1 ± 0.4 μm, respectively, with a percentage error of 6.7%.
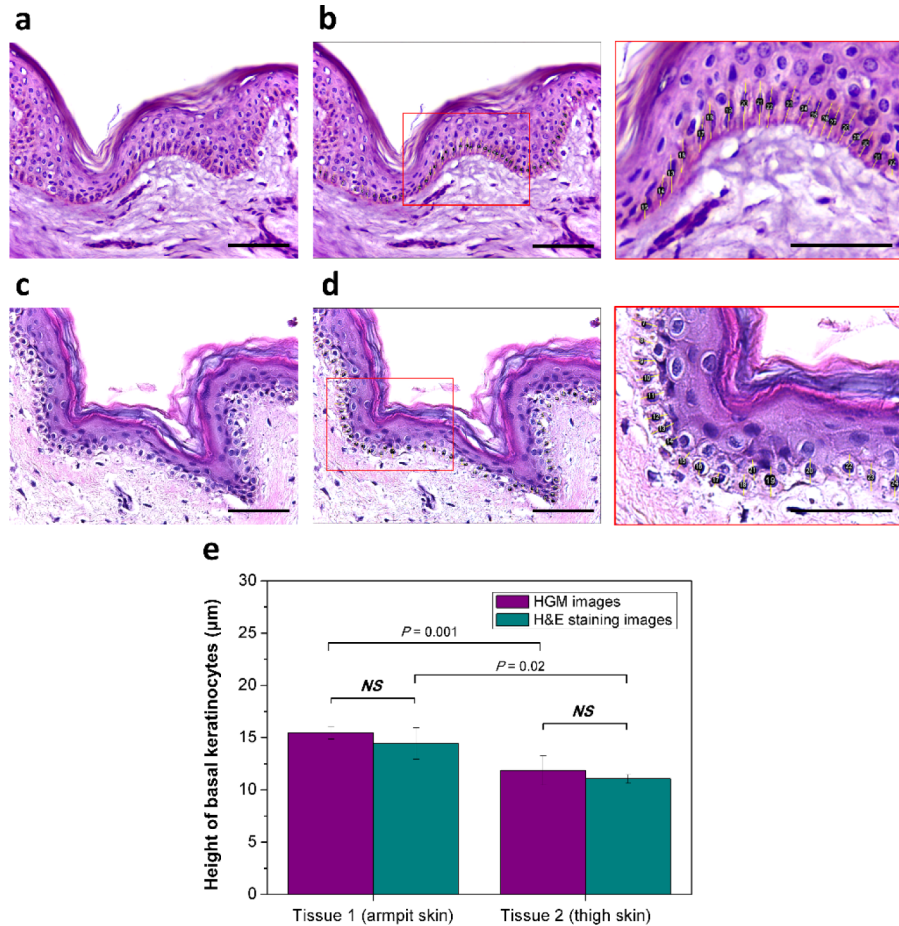

Fig. 5. Hematoxylin and eosin (H&E) staining images of (a, b) normal armpit and (c, d) thigh skin tissues from a 30-year-old woman and an 84-year-old woman, respectively. The mean values of the height of basal keratinocytes from the H&E armpit and thigh skin sections were 15.1 ± 3.1 μm and 10.6 ± 1.5 μm, respectively, as measured using ImageJ software. (e) The ex vivo HBK analysis results from unstained 3D HGM images and H&E staining images. Statistical differences were tested using unpaired t-test. Scale bar = 50 μm. NS: non-significant difference.

3.2. Ex vivo analyses of the HCS of basal keratinocytes

Validation of the HGM system on the basis of the HCS results obtained by *ex vivo* imaging and H&E staining was carried out using skin frozen sections. As shown in Fig. 6(a–d), in the first skin section, the mean HCS in the *ex vivo* HGM images was approximately 62.9 ± 1.5 μm^2, whereas that in the H&E staining images was approximately 65.4 ± 16.2 μm^2, with a percentage

error of 3.9%. For the second section, the mean HCS in the *ex vivo* HGM images was 69.7 ± 4.8 μm^2, whereas that in the H&E staining images was 65.7 ± 24.1 μm^2, with a percentage error of 5.7% [Fig. 6(e–h)].
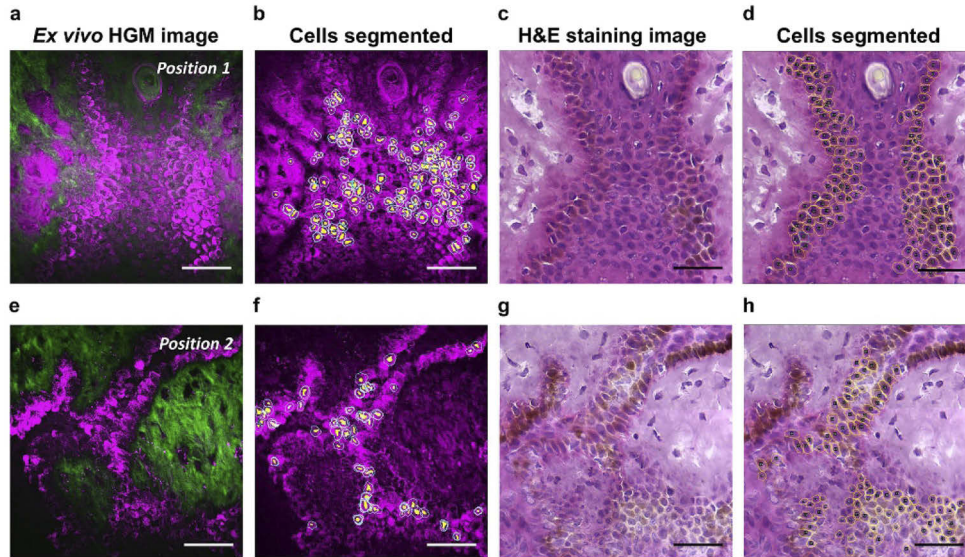

Fig. 6. Comparison of the HCS of basal keratinocytes between ex vivo HGM images and H&E staining images of normal armpit skin specimens from a 47-year-old male volunteer. (a and e) Representative ex vivo HGM images (green: second harmonic generation signal; magenta: third harmonic generation signal). (b and f) The cell nuclei and cytoplasm of the basal keratinocytes were segmented automatically using MATLAB. (c and g) Representative H&E staining images. (d and h) The cell nuclei and cytoplasm of the basal keratinocytes were randomly and manually selected using the ImageJ software. Scale bar = 50 μm. HCS: horizontal cell size; HGM: harmonic generation microscopy; H&E: hematoxylin and eosin.

3.3. In vivo analysis of the HBK

Figure 7(a) shows the comparisons of the average HBK values of all patients between the normal and lesional regions, before and after different laser treatments. Before laser treatment, the HBK in the SLs was significantly higher than that in the normal region for all 25 patients. At baseline, the HBK of the target SLs on the left (mean ± SD: 26.1 ± 3.7 μm) and right cheeks (25.9 ± 3.2 μm) was significantly higher than that of the normal skin (22.2 ± 1.5 μm; P <.001 in both groups, paired t-test). After laser treatment, although there was a significant decrease in the HBK from QSRL treatment (P = .02 at week 3), the value was still significantly higher than that in the normal region on both sides of the face at week 3 (24 ± 2.8 μm for the QSRL-treated region; 23.9 ± 3 μm for the PSNYL-treated region; 22.4 ± 2 μm for the normal region; P = .03 and .05, respectively, paired t-test) and at week 6 (24.1 ± 3.3 for the QSRL-treated region; 24.9 ± 2.7 for the PSNYL-treated region; 22.6 ± 2.6 for the normal region; P = .02 and .002, respectively, paired t-test).

3.4. In vivo analysis of the HCS of basal keratinocytes

No significant difference in HCS values was found between the lesional and normal regions [89.3 ± 7.3 μm^2 for the left side and 90 ± 6.4 μm^2 for the right side in the lesional regions; 90.7 ± 4.5 μm^2 for the normal region; Fig. 7(b)]. After both laser treatments, there was still no
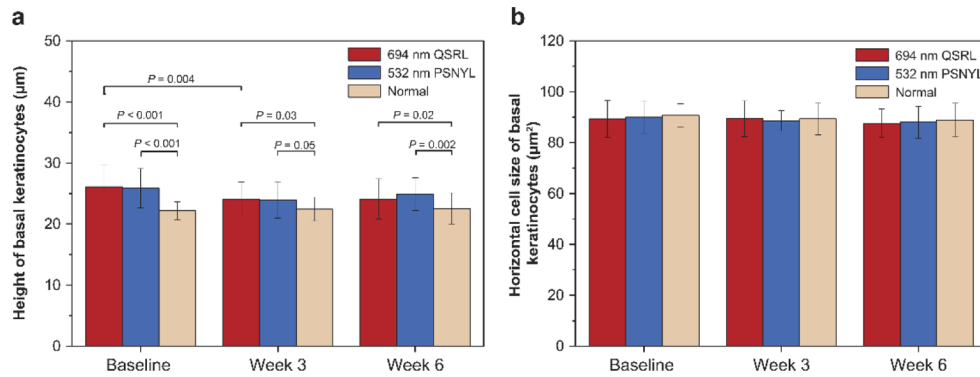
Fig. 7. Morphological parameters relevant to basal keratinocytes. The (a) HBK and (b) HCS of basal keratinocytes were analyzed from the en face in vivo HGM images at baseline, week 3, and week 6. Statistical differences were tested using the paired t-test. PSNYL: picosecond Nd:YAG laser; QSRL: Q-switched ruby laser; HBK: height of basal keratinocytes; HCS: horizontal cell size; HGM: harmonic generation microscopy.

significant difference in HCS values among the different facial regions at week 3 (89.5 ± 7 μm^2 for the QSRL-treated region; 88.6 ± 4 μm^2 for the PSNYL-treated region; 89.4 ± 6.3 μm^2 for the normal region) and at week 6 [87.6 ± 5.6 μm^2 for the QSRL-treated region; 88.1 ± 6.3 μm^2 for the PSNYL-treated region; 88.9 ± 6.6 μm^2 for the normal region; Fig. 7(b)].

4.   Discussion

Using an *in vivo* HGM system before and after laser treatment, we have conducted the slide-free stain-free longitudinal monitoring of two morphological parameters of basal keratinocytes (i.e., HBK and HCS) that are potentially associated with skin senescence in SLs. These parameters have never been analyzed in this way before owing to the technological limitations of other competing *in vivo* imaging systems. Therefore, to our best knowledge, this is the first clinical study to propose remained enlargement of the basal keratinocytes, with a higher HBK but no increase in the HCS, even after laser treatment in 25 Asian patients with SLs. Our results are summarized in Table 1. As pointed out in our previous study, the size of basal keratinocytes (HCS) was associated with intrinsic skin aging and expected to increase with age [21,26].

Previous studies indicated that the pathogenesis of SLs is probably induced by impairment of the cellular proliferation and differentiation programs in SLs [27]. Expression of the Ki-67 protein, a marker of keratinocyte proliferation, was observed to be lower in SLs [28]. Lin *et al.* [29] reported that Ki-67 expression was higher in the early-mid stages of SLs development and decreased in the late stage. Moreover, filaggrin and involucrin, both markers of keratinocyte differentiation, are also expressed in low amounts in SLs lesions [30]. Therefore, such slowed cellular proliferation and differentiation could lead to the quiescence of enlarged senescent keratinocytes, resulting in the observed higher HBK in SLs. Herein, we propose that a high HBK value could be a potential hallmark parameter for characterizing the malfunctioned proliferation and differentiation of basal cells in SLs. Even though the treatment might reduce the abnormal HBK height, after either laser treatment, the HBK of SLs lesions remain significantly higher than normal. Combining this finding with the results of other melanin clearance studies [31,32], we surmise that laser depigmentation treatment removes excess melanin but lacks the ability to completely treat the impairments of proliferation and differentiation in SLs. Consequently, the height of melanin-loaded keratinocytes remains high, rendering the deposition of melanosomes easy, which could result in the recurrence of SLs or imperfect treatment outcomes [33,34].

Table 1. HBK and HCS analysis results of the in vivo and ex vivo experiments.

	HGM images	H&E staining images	Percentage error
***Ex vivo* analyses of the HBK (μm)**			
Tissue 1 (thigh skin)	15.5 ± 0.7	14.5 ± 1.5	6.5%
Tissue 2 (armpit skin)	11.9 ± 1.5	11.1 ± 0.4	6.7%
***Ex vivo* analyses of the HCS of basal keratinocytes (μm^2)**			
Skin specimens 1 (armpit skin)	62.9 ± 1.5	65.4 ± 16.2	3.9%
Skin specimens 2 (armpit skin)	69.7 ± 4.8	65.7 ± 24.1	5.7%
	Baseline	**Week 3**	**Week 6**
***In vivo* analysis of the HBK (μm)**			
Left Cheeks (694-nm QSRL)	26.1 ± 3.7	24 ± 2.8	24.1 ± 3.3
Right Cheeks (532-nm QSRL)	25.9 ± 3.2	23.9 ± 3	24.9 ± 2.7
Normal regions	22.2 ± 1.5	22.4 ± 2	22.6 ± 2.6
***In vivo* analysis of the HCS of basal keratinocytes (μm^2)**			
Left Cheeks (694-nm QSRL)	89.3 ± 7.3	89.5 ± 7	87.6 ± 5.6
Right Cheeks (532-nm QSRL)	90 ± 6.4	88.6 ± 4	88.1 ± 6.3
Normal regions	90.7 ± 4.5	89.4 ± 6.3	88.9 ± 6.6

Among all the non-invasive label-free imaging techniques, optical coherence tomography (OCT) can be used to obtain histopathological skin images with high penetration capability. However, because OCT lacks spatial resolution, cellular information on the keratinocytes in SLs cannot be acquired with this imaging method [35]. Although reflection confocal microscopy (RCM) may seem to be another attractive choice, as it provides images with a better resolution and strong contrast owing to the high refractive index of melanin, the limited resolution at the dermal-epidermal junction still causes the blurred contouring of cells, especially when imaging those of hyperpigmented skin disorders [35–37]. Hence, studies that have used RCM to observe changes in the melanin content have not used the method to further investigate the morphological parameters of basal keratinocytes in SLs. HGM, which combines nonlinear THG and SHG signals to render high spatial resolutions, have already been proposed for the quantitative analysis of cellular morphometries [23,38,39]. Moreover, the 1260 nm central wavelength used in HGM minimizes the tissue scattering, avoids the melanin absorption, and fits within the optical window of human skin, thus allowing for a high penetration depth and thereby better acquisition of the morphometrics of the various skin cell layers [40]. Importantly, we have validated the HGM system through *ex vivo* analyses, verifying that it can provide not only HCS but also HBK results equivalent to those obtained by H&E staining. The limitations of this study include the small number of patients and a short period of follow-up.

5. Conclusion

This study demonstrated the feasibility of *in vivo* HGM for the longitudinal monitoring of basal keratinocytes in SLs and the potential use of the HBK as a novel clinical parameter for characterizing the malfunctioned proliferation and differentiation of these cells. Here, we disclosed the protocol for the analysis of the HBK through *en face* HGM image stacks and validated its correctness through comparison with the gold standard H&E samples. Moreover, we propose that the HBK mostly remains abnormal after both types of laser treatment and might lead to the recurrence of SLs or imperfect appearance outcomes.

References

1. S. B. Rahman and J. Bhawan, "Lentigo," Int. J. Dermatol. **35**(4), 229–239 (1996).
2. J. Nip, S. Potterf, S. Rocha, S. Vora, and C. Bosko, "The new face of pigmentation and aging," in *Textbook of Aging Skin* (Springer, 2010), pp. 509–521 (2010).
3. D. Kopera, U. Hohenleutner, and M. Landthaler, "Quality-switched ruby laser treatment of solar lentigines and Becker's nevus: a histopathological and immunohistochemical study," Dermatology **194**(4), 338–343 (1997).
4. A. Sadighha, S. Saatee, and G. Muhaghegh-Zahed, "Efficacy and adverse effects of Q-switched ruby laser on solar lentigines: a prospective study of 91 patients with Fitzpatrick skin type II, III, and IV," Dermatol. Surg. **34**(11), 1465–1468 (2008).
5. T. Kono, D. Manstein, H. H. Chan, M. Nozaki, and R. R. Anderson, "Q-switched ruby versus long-pulsed dye laser delivered with compression for treatment of facial lentigines in Asians," Laser Surg. Med. **38**(2), 94–97 (2006).
6. K. Negishi, H. Akita, S. Tanaka, Y. Yokoyama, S. Wakamatsu, and K. Matsunaga, "Comparative study of treatment efficacy and the incidence of post-inflammatory hyperpigmentation with different degrees of irradiation using two different quality-switched lasers for removing solar lentigines on Asian skin," J. Eur. Acad. Dermatol. **27**(3), 307–312 (2013).
7. D. C. Wu, M. P. Goldman, H. Wat, and H. H. Chan, "A systematic review of picosecond laser in dermatology: evidence and recommendations," Laser Surg. Med. **53**(1), 9–49 (2021).
8. J. P. Ortonne, A. G. Pandya, H. Lui, and D. Hexsel, "Treatment of solar lentigines," J. Am. Acad. Dermatol. **54**(5), S262–S271 (2006).
9. C. Kaminaka, F. Furukawa, and Y. Yamamoto, "The clinical and histological effect of a low-fluence Q-switched 1,064-nm neodymium: yttrium-aluminum-garnet laser for the treatment of melasma and solar lentigenes in Asians: prospective, randomized, and split-face comparative study," Dermatol. Surg. **43**(9), 1120–1133 (2017).
10. H. J. Kang, J. I. Na, J. H. Lee, M. R. Roh, J. Y. Ko, and S. E. Chang, "Postinflammatory hyperpigmentation associated with treatment of solar lentigines using a Q-Switched 532-nm Nd: YAG laser: a multicenter survey," J. Dermatol. Treat. **28**(5), 447–451 (2017).
11. M. Bastiaens, J. Hoefnagel, R. Westendorp, B. J. Vermeer, and J. N. Bouwes Bavinck, "Solar lentigines are strongly related to sun exposure in contrast to ephelides," Pigment Cell Res **17**(3), 225–229 (2004).
12. C. Praetorius, R. A. Sturm, and E. Steingrimsson, "Sun-induced freckling: ephelides and solar lentigines," Pigm. Cell. Melanoma R. **27**(3), 339–350 (2014).
13. W. J. Lee, S. Y. Jo, M. H. Lee, C. H. Won, M. W. Lee, J. H. Choi, and S. E. Chang, "The effect of MCP-1/CCR2 on the proliferation and senescence of epidermal constituent cells in solar lentigo," Int. J. Mol. Sci. **17**(6), 948 (2016).
14. J. Shin, J. Y. Park, S. Kim, and H. Kang, "Characteristics of keratinocytes in facial solar lentigo with flattened rete ridges: comparison with melasma," Clin. Exp. Dermatol. **40**(5), 489–494 (2015).
15. Y. Soroka, Z. Ma'or, Y. Leshem, L. Verochovsky, R. Neuman, F. M. Brégégère, and Y. Milner, "Aged keratinocyte phenotyping: morphology, biochemical markers and effects of Dead Sea minerals," Exp. Gerontol. **43**(10), 947–957 (2008).
16. S. Y. Chen, S. U. Chen, H. Y. Wu, W. J. Lee, Y. H. Liao, and C. K. Sun, "In vivo virtual biopsy of human skin by using noninvasive higher harmonic generation microscopy," IEEE J. Sel. Top. Quant. **16**(3), 478–492 (2010).
17. T. M. Liu, S. W. Chu, C. K. Sun, B. L. Lin, P. C. Cheng, and I. Johnson, "Multiphoton confocal microscopy using a femtosecond Cr: forsterite laser," Scanning **23**(4), 249–254 (2001).
18. S. Chakraborty, S. T. Chen, Y. T. Hsiao, M. J. Chiu, and C. K. Sun, "Additive-color multi-harmonic generation microscopy for simultaneous label-free differentiation of plaques, tangles, and neuronal axons," Biomed. Opt. Express **11**(2), 571–585 (2020).
19. Y. H. Ho, Y. Pan, C. K. Sun, and Y. H. Liao, "Presence of intralesional melanocytes as a histopathological feature of actinic keratosis based on in vivo harmonic generation microscopy in Asians," Photodermatol Photoimmunol Photomed **37**(1), 20–27 (2021).
20. J. H. Lai, E. Y. Liao, Y. H. Liao, and C. K. Sun, "Investigating the optical clearing effects of 50% glycerol in ex vivo human skin by harmonic generation microscopy," Sci. Rep. **11**(1), 1–14 (2021).
21. Y. H. Liao, Y. H. Su, Y. T. Shih, W. S. Chen, S. H. Jee, and C. K. Sun, "In vivo third-harmonic generation microscopy study on vitiligo patients," J. Biomed. Opt. **25**(1), 014504 (2020).
22. C. K. Sun and S. Y. Chen, "Vacuum-pump sucker," U.S. Patent 9795340B2 (2017).
23. Y. H. Liao, S. Y. Chen, S. Y. Chou, P. H. Wang, M. R. Tsai, and C. K. Sun, "Determination of chronological aging parameters in epidermal keratinocytes by in vivo harmonic generation microscopy," Biomed. Opt. Express. **4**(1), 77–88 (2013).

24. G. G. Lee, H. H. Lin, M. R. Tsai, S. Y. Chou, W. J. Lee, Y. H. Liao, C. K. Sun, and C. F. Chen, "Automatic cell segmentation and nuclear-to-cytoplasmic ratio analysis for third harmonic generated microscopy medical images," IEEE Trans. Biomed. Circuits Syst **7**(2), 158–168 (2013).

25. K. M. Halprin, "Epidermal "Turnover Time"—A Re-Examination," Br. J. Dermatol. **86**(1), 14–19 (1972).

26. K. H. Lin, Y. H. Liao, M. L. Wei, and C. K. Sun, "Comparative analysis of intrinsic skin aging between Caucasian and Asian subjects by slide-free in vivo harmonic generation microscopy," J. Biophotonics **13**(4), e201960063 (2020).

27. M. J. Barysch, R. P. Braun, I. Kolm, V. Ahlgrimm-Siesz, R. Hofmann-Wellenhof, C. Duval, E. Warrick, F. Bernerd, S. Nouveau, and R. Dummer, "Keratinocytic malfunction as a trigger for the development of solar lentigines," Dermatopathology **6**(1), 1–11 (2019).

28. N. Ünver, P. Freyschmidt-Paul, S. Hörster, H. Wenck, F. Stäb, T. Blatt, and H. P. Elsässer, "Alterations in the epidermal–dermal melanin axis and factor XIIIa melanophages in senile lentigo and ageing skin," Brit. J. Dermatol. **155**(1), 119–128 (2006).

29. C. B. Lin, Y. Hu, D. Rossetti, N. Chen, C. David, A. Slominski, and M. Seiberg, "Immuno-histochemical evaluation of solar lentigines: The association of KGF/KGFR and other factors with lesion development," J. Dermatol. Sci. **59**(2), 91–97 (2010).

30. H. Aoki, O. Moro, H. Tagami, and J. Kishimoto, "Gene expression profiling analysis of solar lentigo in relation to immunohistochemical characteristics," Br J Dermatol **156**(6), 1214–1223 (2007).

31. C. E. Jones and K. Nouri, "Laser treatment for pigmented lesions: a review," J Cosmet Dermat **5**(1), 9–13 (2006).

32. Z. Bukvić Mokoš, J. Lipozenčić, A. Pašić, and I. Fattorini, "Laser therapy for solar lentigines: review of the literature and case report," Acta Dermatovener. Cr. **14**(2), 81 (2006).

33. P. K. Lee, C. N. Rosenberg, H. Tsao, and A. J. Sober, "Failure of Q-switched ruby laser to eradicate atypical-appearing solar lentigo: report of two cases," J. Am. Acad. Dermatol. **38**(2), 314317 (1998).

34. P. Bjerring and K. Christiansen, "Intense pulsed light source for treatment of small melanocytic nevi and solar lentigines," J. Cutan. Laser Ther. **2**(4), 177–181 (2000).

35. T. Yamashita, K. Negishi, T. Hariya, N. Kunizawa, K. Ikuta, M. Yanai, and S. Wakamatsu, "Intense pulsed light therapy for superficial pigmented lesions evaluated by reflectance-mode confocal microscopy and optical coherence tomography," J. Invest. Dermatol. **126**(10), 2281–2286 (2006).

36. R. G. Langley, E. Burton, N. Walsh, I. Propperova, and S. J. Murray, "In vivo confocal scanning laser microscopy of benign lentigines: comparison to conventional histology and in vivo characteristics of lentigo maligna," J. Am. Acad. Dermatol. **55**(1), 88–97 (2006).

37. M. Rajadhyaksha, M. Grossman, D. Esterowitz, R. H. Webb, and R. R. Anderson, "In vivo confocal scanning laser microscopy of human skin: melanin provides strong contrast," J. Invest. Dermatol. **104**(6), 946–952 (1995).

38. M. R. Tsai, Y. H. Cheng, J. S. Chen, Y. S. Sheen, Y. H. Liao, and C. K. Sun, "Differential diagnosis of nonmelanoma pigmented skin lesions based on harmonic generation microscopy," J. Biomed. Opt. **19**(3), 036001 (2014).

39. Y. H. Liao, W. C. Kuo, S. Y. Chou, C. S. Tsai, G. L. Lin, M. R. Tsai, Y. T. Shih, G. G. Lee, and C. K. Sun, "Quantitative analysis of intrinsic skin aging in dermal papillae by in vivo harmonic generation microscopy," Biomed. Opt. Express **5**(9), 3266–3279 (2014).

40. R. R. Anderson and J. A. Parrish, "The optics of human skin," J. Invest. Dermatol. **77**(1), 13–19 (1981).